Accepted Manuscript

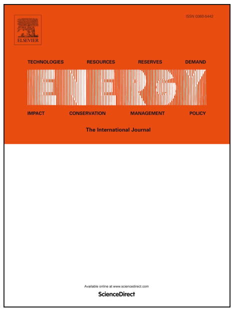

Effect of cooling system design on the performance of the recompression CO_2 cycle for concentrated solar power application

M. Monjurul Ehsan, Sam Duniam, Jishun Li, Zhiqiang Guan, Hal Gurgenci, Alexander Klimenko

PII: S0360-5442(19)30988-0

DOI: https://doi.org/10.1016/j.energy.2019.05.108

Reference: EGY 15360

To appear in: *Energy*

Received Date: 19 December 2018

Revised Date: 14 May 2019

Accepted Date: 15 May 2019

Please cite this article as: Ehsan MM, Duniam S, Li J, Guan Z, Gurgenci H, Klimenko A, Effect of cooling system design on the performance of the recompression CO_2 cycle for concentrated solar power application, *Energy* (2019), doi: https://doi.org/10.1016/j.energy.2019.05.108.

This is a PDF file of an unedited manuscript that has been accepted for publication. As a service to our customers we are providing this early version of the manuscript. The manuscript will undergo copyediting, typesetting, and review of the resulting proof before it is published in its final form. Please note that during the production process errors may be discovered which could affect the content, and all legal disclaimers that apply to the journal pertain.

ACCEPTED MANUSCRIPT

Effect of Cooling System Design on the Performance of the Recompression CO_2 Cycle for Concentrated Solar Power Application

M. Monjurul Ehsan[a,]*, Sam Duniam[a], Jishun Li[b], Zhiqiang Guan[a], Hal Gurgenci[a], Alexander Klimenko[a]

[a]School of Mechanical and Mining Engineering
The University of Queensland, Brisbane, QLD 4072, Australia.
[b]School of Mechatronics Engineering
Henan University of Science and Technology, Luoyang, Henan, China 471003.

Abstract

The thermal performance of a supercritical CO_2 (sCO_2) recompression cycle is expressively influenced by main compressor inlet temperature. Design of the cooling system is imperative since the compressor inlet temperature substantially influence the system performance. Due to nonlinear variation of both thermal and transport properties of the CO_2 under critical condition, the cooling tower design and selection for the sCO_2 cycle power plant is quite different from the power plants with steam cycle. The present work comprehensively investigates the effect of cooling system design on the optimal cycle performance under different operating condition. An iterative section method is applied while designing and optimizing the air-cooled heat exchanger bundles inside the tower. Prior to the design of natural draft dry cooling tower (NDDCT), an optimal operating condition is rectified at which the cycle efficiency is maximal. The tower performance is investigated by demonstrating unit height heat rejection and average heat rejection by each heat exchanger bundle. A detailed economic analysis of NDDCT is performed which takes account of capital cost, maintenance cost, annual cost, and specific investment cost. The thermo-economic assessment of the NDDCT is conducted by the influence of sCO_2 inlet temperature inside the tower and variation of ambient air.

Keywords: supercritical CO_2; cooling tower; heat exchanger; concentrated solar; recompression cycle.

Corresponding Author: M. Monjurul Ehsan, Tel: +61423849284
Email address: m.ehsan@uqconnect.edu.au

Highlights

- Detailed modelling of NDDCT coupled with the recompression sCO_2 cycle.
- Implementation of iterative section method for sCO_2 heat exchanger unit.
- Detailed economic analysis of NDDCT.
- Impact of variant sCO_2 and air temperature on the system performance.
- Exergy and component-wise irreversibility analysis.

ACCEPTED MANUSCRIPT

ACCEPTED MANUSCRIPT

1. Introduction

The closed-loop Brayton cycle with supercritical CO_2 (sCO_2) as working fluid is proposed as the next generation advanced power cycle for applications as diverse as nuclear, clean coal, geothermal and concentrating solar thermal [1, 2]. In contrast with the conventional superheated/supercritical Rankine cycle, this sCO_2 Brayton cycle provides simple cycle layout and improved thermal efficiency at the same turbine inlet condition [3]. The sCO_2 power cycle can significantly lessen the overall cost of the solar power plant due to its thermal efficiency being higher than steam at moderate turbine inlet temperatures (500-600^oC) and its suitability for very high temperatures where steam is no longer an option [4]. The cooling system is a critical component in sCO_2 power plants. The cooling process in the sCO_2 Brayton cycle occurs near the critical condition. The nonlinear and sharp variation of sCO_2 properties poses a unique heat exchanger design problem not encountered with the constant property fluids [5].

1.1 Studies on Power Cycles

Thermodynamic analysis of different sCO_2 power cycle options (recuperative cycle, recompression cycle, and partial cooling cycle) showed that, with judicious process design, thermal efficiencies over 50% are achievable [1]. A compressor inlet temperature of 45^0C and 60^0C is generally considered by assuming dry cooling. Numerical modelling and prototype lab-scale experimentation were conducted by Iverson et al. [6] to assess the transient behavior of the recompression cycle. Various studies identified several advantages of sCO_2 power cycles over the steam Rankine cycle. The compact equipment due to high-pressure fluid density, lower specific volume and simple plant design of sCO_2 cycle place it as the alternative to the traditional steam cycle for large-scale electricity generation [7, 8]. Garg et al. [9] outlined the advantages of the sCO_2 cycle over the subcritical and transcritical CO_2 cycle by investigating the thermal efficiency, specific work and irreversibility analysis. Conboy et al. [10] conducted a small-scale experiment with a 20 kW simple Brayton cycle and investigated the dynamic performance of the printed circuit recuperator, the primary heat exchanger, and the turbo-machineries. Ehsan et al. [11] reviewed the Nusselt number and pressure drop correlations applicable for sCO_2 in a circular tube. The heat transfer characteristics of sCO_2 during the cooling process was comprehensively discussed. Xu et al. [12] reported comprehensive design strategies of sCO_2 power cycles for traditional coal-fired power application by investigating the influence of reheating and intercooling.

1.2 Power Cycle Application in CSP

Sulaiman and Atif [13] performed a comparative study of five different sCO_2 power cycles integrated with solar power tower. The fluctuation of power outputs was reported at various seasonal times, indicating the importance of the cooling system design in air-cooled power generators. The implementation of sCO_2 as both heat transfer fluid and working fluid was proposed for solar tower application by demonstrating the advantages of sCO_2 over the synthetic oil, molten salts, and steam generation [14]. Zhu et al. [15] compared the thermal performance of various sCO_2 power cycles in CSP with regards to cycle highest temperature and recuperator conductance. Wang and He [16] compared the performance of different sCO_2 power cycles integrated with the molten salt central receiver. The comparison performed in terms of specific work, system efficiency, and receiver performance [17]. Binotti et al. [18] developed a central receiver high-temperature solar tower model to optimize the power cycles. Milani et al. [19, 20]

ACCEPTED MANUSCRIPT

reported the control strategies and dynamic simulation of solar driven sCO_2 recompression cycle and comparison performed between the direct and indirect configuration of solar heat input.

1.3 Studies on Dry Cooling for sCO_2 Cycle

In concentrated solar application, the research on the dry cooling option is receiving attention since the sCO_2 power cycle can yield higher cycle efficiency at a moderate climate condition. Conboy et al. [21] explored the compatibility dry cooling option for sCO_2 power cycle for nuclear reactor application. Thermal efficiency was better than steam cycle when the reactor temperature exceeded 550^0C. Dyreby et al. [22] optimized the pressure ratio of a simple and recompression cycle by assuming dry cooling in CSP application. At higher ambient temperatures, increasing the compressor inlet pressure helped to maintain the design-point thermal efficiency. Padilla et al. [23, 24] performed the detailed irreversibility analysis of four different sCO_2 power cycles with dry cooling. Main compression cycle with intercooling showed the maximum thermal efficiency of 55% at 850^0C. Moisseytsev and Sienicki [25] proposed a finned type shell and tube heat exchanger cooled by water flowing on the shell-side and sCO_2 in tube side in a supercritical recompression cycle. The number of tubes and pitch ratio was optimized. Ho et al. [26] studied the thermo-economic analysis of different power cycles by considering the cooling system as a finned tube heat exchanger unit. Battisti et al. [27] conducted a comprehensive system optimization of a recompression cycle with single reheating and dry cooling. Li et al. conducted experiments with a 20 kW condensing CO_2 cycle using an air-cooled condenser. Milani et al. [20], Luu et al. [28], Ma et al. [14], Son and Lee [29] and Zeyghami and Khalili [30] studied various aspects of the dry-cooled supercritical CO_2. Duniam et al. [31] conducted the preliminary analysis of the direct and indirect dry cooling system for the sCO_2 recompression cycle. In our previous work, we developed a well-validated MATLAB code to model a NDDCT for 25 MW solar thermal power plant [32, 33]. In these studies, common geometric relations for the tower geometry were used in order to conduct a preliminary investigation of the direct and indirect cooling system.

1.4 Research Scope

In all of these past studies on dry cooling of sCO_2 power generating systems, the air-cooling system was included as a black box. Its physical size and design details were not mentioned. This research gap is addressed by investigating the modelling of a natural draft dry cooling tower (NDDCT) integrated with the sCO_2 recompression cycle. Although, the cooling potential of a dry cooling unit is restricted by the dry bulb temperature of the air and less efficient than wet coolers, natural draft dry cooling tower (NDDCT) is preferred as a cooling system in sCO_2 power cycles due to inadequate water supply and no maintenance and electricity cost associated with mechanical fans [34, 35].

The present work takes the line of previous work further and optimizes the NDDCT in the context of influence on power cycle thermal performance. The requirements for an efficient cooling system in the sCO_2 cycle is to cool sCO_2 to a desired compressor inlet temperature at which the cycle provides the maximum efficiency. Dry cooling using a NDDCT is adapted and its impact on the system performance is analyzed. The abrupt property changes of the sCO_2 near the critical point is a challenge in designing such cooling systems. This is addressed by discretizing the heat exchangers and analyzing the heat exchange process in segments. The thermal assessment of the power cycle is investigated by calculating several performance indicators (cycle efficiency, exergy efficiency, cooling efficiency, and irreversibility analysis).

The required specification of NDDCT is revealed for various capacities of power plant (40 MW, 60 MW, 80 MW, and 100 MW). The economic analysis of NDDCT is also performed in terms of capital cost, maintenance cost, annual cost, and specific investment cost.

2. Power Cycle Modelling and Validation

A recompression cycle is modelled coupled with the NDDCT as shown in **Fig. 1**. The pinch point problem of simple Brayton cycle is avoided by using two recuperators. The thermal energy is added to the primary heat exchanger to attain the desired turbine inlet temperature. The hot turbine exhaust transfers some of its sensible heat to the return stream in the HTR and LTR. The stream at the LTR outlet of the low-pressure side is split into two. One path goes to the NDDCT where the sCO_2 stream is cooled to the desired sCO_2 outlet temperature by the air-cooled heat exchanger bundles inside the NDDCT. The other stream is compressed by the RC compressor and mixes with the outflow from the LTR at high-pressure side. The ratio of the NDDCT flow rate to the RC flow rate is referred to as the split ratio, SR. The split ratio is varied at different operating conditions in order to satisfy the constraint of the pinch point temperature of $5^{o}C$ set at the recuperators. Following are the assumptions made during NDDCT and power cycle modelling.

(a) All components are completely insulated.
(b) The heat exchange occurs under a steady state condition.
(c) The changes in potential and kinetic energy of the fluid are neglected.
(d) A constant pressure drop of 20 kPa is assumed for the recuperators.
(e) Expanders and compressors have constant isentropic efficiencies
(f) At various air ambient temperatures, the thermal energy added to the primary heat exchanger is a variable so that the desired turbine inlet temperature is reached. This is a realistic assumption for a sCO_2 power cycle being heated from the CSP thermal storage.
(g) At the LTR high-pressure outlet, the two mixing sCO_2 streams have the same temperature.
(h) All other assumptions during modelling of NDDCT are taken from ref [36].

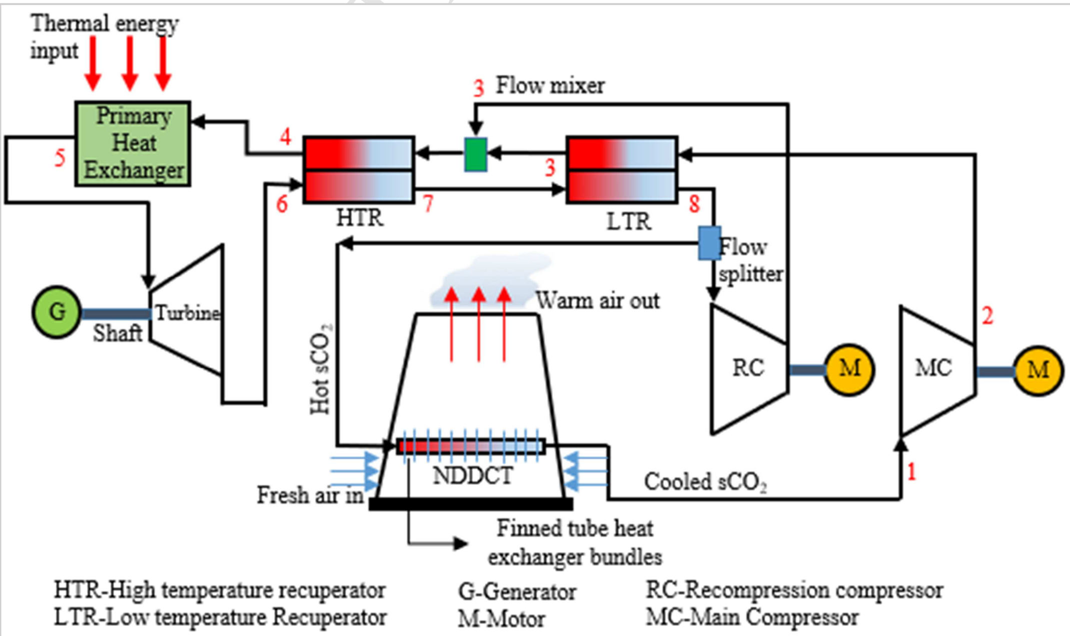

Fig. 1. The Recompression cycle coupled with NDDCT.

The power cycle is modelled using IPSEpro, a process simulation software [37]**.** The standard modules are used for all components except the NDDCT. The results are validated against the available literature (Dostal et al. [38], Turchi et al. [1] and Besarati and Goswami [39]). In these papers, the turbine and compressor isentropic efficiencies were taken as 90% and 89%, respectively. They modelled the recuperator using a heat exchanger effectiveness of 95%. We will represent it using a pinch point temperature difference of 5^{o}C and equal temperature differential of the sCO_2 streams at both sides of the recuperator. The cycle maximum and minimum pressures were taken as 25 MPa and 7.4 MPa, respectively. The lowest temperature of the cycle was set to 32^{o}C and cycle thermal efficiency was evaluated for a range of turbine inlet temperature of 500^{o}C to 850^{o}C. The results agree with the literature, as shown in **Table 1,** for turbine inlet temperatures up to 650^{o}C. At higher turbine inlet temperatures, the present analysis predicts higher values in efficiency. This is due to the assumption made while modelling the recuperators. **Table 2** shows the design point operating conditions at which the NDDCT is designed. These parameters are chosen based on the optimum operating conditions, as described in section 3, at which the cycle provides the highest thermal efficiency and from the existing literature.

Table 1. Validation of present work with recompression cycle.

Parameter	Cycle thermal efficiency (%)						
Turbine inlet temperature (^{0}C)	Dostal et al.	% of error	Turchi et al.	% of error	Besarati and Goswami	% of error	Present work
500	0.438	0.458	0.437	0.229	0.441	0.917	0.436
550	0.462	0.434	0.462	0.478	0.462	0.478	0.461
600	0.482	0.001	0.484	0.414	0.482	0.004	0.482
650	0.501	0.398	0.504	0.398	0.502	0.003	0.502
700	0.514	1.153	0.521	0.192	0.518	0.384	0.521
750	0.528	1.675	0.534	0.558	0.531	1.303	0.537
800	0.541	1.818	0.548	0.363	0.544	1.909	0.551
850	0.551	2.482	0.56	0.709	0.558	1.063	0.564

Table 2. Design point parameters for cycle modelling.

Parameter	Value
Plant thermal output, W_{net}	40MW, 60MW, 80MW and 100 MW
Adiabatic efficiency of turbine, η_T	0.93
Adiabatic efficiency of compressor, η_C	0.89
Mechanical efficiency, η_M	1.0
Cycle split ratio, *SR*	61%
Turbine inlet temperature, TIT	650^{o}C
Inlet temperature of NDDCT	67^{o}C
Desired cycle lowest temperature, *CIT*	33^{o}C
Ambient air properties	20^{o}C, 1 m/s, 0.1MPa
The relative humidity of air, R_H	60 %
Cycle higher pressure, P_H	20MPa
Cycle lower pressure, P_L	8 MPa
LTR pinch point temperature	5^{o}C
Pressure drop in HTR and LTR	20 kPa

3. Preliminary Assessment of Power Cycle

ACCEPTED MANUSCRIPT

The effect of cycle pressure ratio on the η is shown in **Fig. 2**, by setting the cycle lower pressure at 8 MPa and increasing the higher pressure from 12 MPa to 20 MPa. The input parameters are taken from table 2. The η sharply decreases with the increase of the main compressor inlet temperature. However, for the range of cycle pressure ratio X_p=1.5-1.9, the η initially increases with the compressor inlet temperature with a range of 30°C to 35°C. For a higher range of cycle pressure ratio (X_p=2.1-2.5), the η keeps increasing up to the compressor inlet temperature of 33°C. This unique phenomenon at lower CIT occurs due to the variation of the transport properties of the working fluid in the region of the pseudocritical temperature. Obviously, the cycle performance increases with higher cycle pressure ratio. The influence of the cycle pressure ratio on the W_{net} at various compressor inlet temperature is also demonstrated. As expected, the W_{net} decreases with the increase of the compressor inlet temperature. As the pressure is lowered, more heat is extracted from the heat source and more work (W_{net}) is generated but this comes at the cost of lower efficiency.

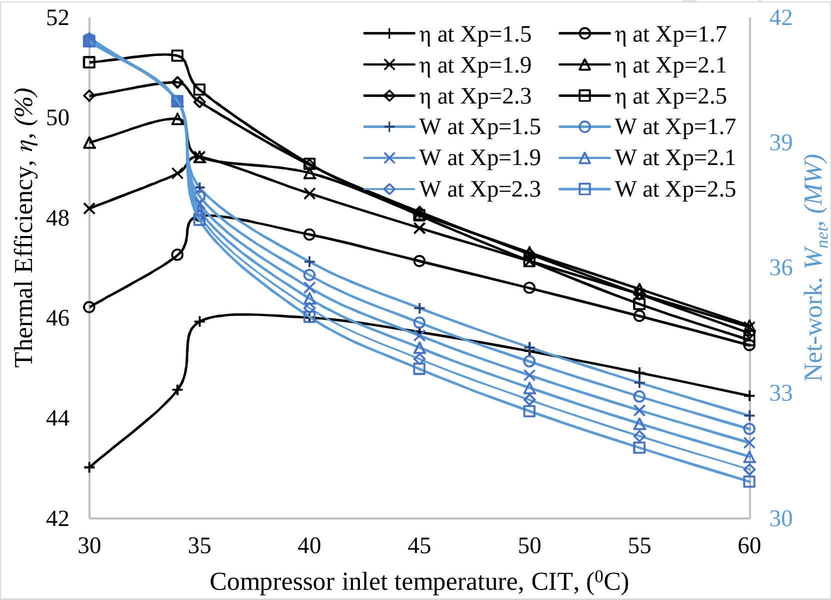

Fig. 2. Effect of cycle pressure ratio on thermal performance and net power generation at various CIT.

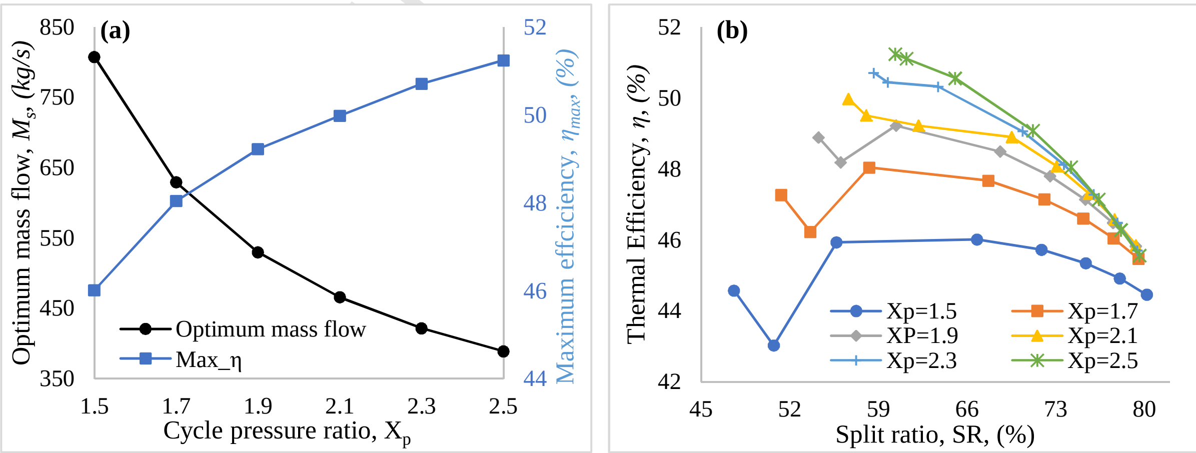

Fig. 3. Effect of cycle pressure ratio on (a) cycle mass flow rate and (b) cycle *SR* on η.

Fig. 3(a) shows the optimum cycle mass flow rate at various cycle pressure ratios. Increasing the pressure ratio decreases the cycle mass flow rate proportionally. The corresponding maximum η obtained with various cycle pressure ratio is also shown in the figure. The **Fig. 3(b)** shows the influence of the *SR* on the cycle performance at various pressure ratios. Six values of SR were used to generate each curve in **Fig. 3(b).** Each SR value is computed by an optimization process performed at a different compressor inlet temperature, as this temperature is varied from 30°C to 60°C. For lower pressure ratio cases (X_p=1.5-1.9), the η is maximum at comparatively lower *SR* but the efficiency falls when the SR is further increased. At high-pressure ratios (X_p=2.1-2.5), the maximum η is observed at the lowest *SR* possible. The selected *SR* for each operating condition set is always maintained by the cycle itself in order to comply with the boundary condition set at the recuperators. Based on the maximum efficiency achieved at X_p=*2.5* indicated in **Fig. 3(a)**, therefore, the power cycle integrated with NDDCT is modelled with a cycle higher pressure of 20 MPa and lower pressure of 8 MPa.

4. Design Methodology of NDDCT

4.1 Thermodynamics of NDDCT

In the present work, NDDCT is employed as a cooling component in the sCO_2 power cycle. Finned tube heat exchanger bundles are installed with horizontal orientation at the tower inlet. The draft force generated owing to the density variance between the hot air inside and the colder air outside makes the ambient air flow through the heat exchangers, remove the heat from hot sCO_2 flowing through the tubes, and rise through the tower without needing fans. In arid areas, the use of NDDCT can significantly lessen energy consumption as there are no parasitic losses compared to mechanical draft cooling. Operation and maintenance costs are also lower and there are no environmental concerns because corrosion, scale deposition and the water loss normally associated with evaporative cooling are not relevant. However, the cooling efficiency is restricted by the dry bulb temperature of the air. **Fig. 4** shows the features of NDDCT with heat exchanger bundles arranged horizontally. In the present work, the NDDCT is designed at 20°C air temperature with 60% relative humidity and wind velocity of 1 m/s. The cooling potential of NDDCT is significantly influenced by the tower geometry, the specification of the heat exchanger and the ambient air properties. Dry adiabatic lapse rate (DALR) is taken as 0.000975 Km^{-1}. The calculation of air properties at various positions of the tower is shown in **Table 3**. Yoon et al. [40] correlation is used to calculate the local Nusselt number, Nu_s of sCO_2 applicable for macro tube geometries.

$$Nu_s = aRe_s{}^b Pr_s{}^c \left(\frac{\rho_{pc}}{\rho_s}\right)^n \quad (1)$$

The overall conductance, *UA* value of the heat exchanger is expressed by,

$$UA = [\frac{1}{(h_s A_s)} + \frac{1}{2\pi k_t n_b n_{tb} L} ln\frac{d_o}{d_i} + \frac{1}{2\pi k_f n_b n_{tb} L} ln\frac{d_f}{d_o} + \frac{1}{(h_a e_f A_{aT})}]^{-1} \quad (2)$$

The temperature correction factor, F_T is determined by

$$F_T = 1 - \sum_{i=1}^{4}\sum_{k=1}^{4} a_{i,k}(1-\varphi_3)^k \sin\left[2iarctan\left(\frac{\varphi_1}{\varphi_2}\right)\right] \quad (3)$$

$$\varphi_1 = \frac{(T_{si}-T_{so})}{(T_{si}-T_{a3})};\ \varphi_2 = \frac{(T_{a4}-T_{a3})}{(T_{si}-T_{a3})};\ \varphi_3 = \frac{(\varphi_1-\varphi_2)}{\ln[\frac{(\varphi_1-\varphi_2)}{(1-\varphi_2)/(1-\varphi_1)}]}$$

Various types of flow resistances are encountered by the air stream inside the NDDCT [36]. The cooling tower supports exert some losses, K_{ts} while the air stream flows at the base of the tower, from state 1 to 2. The tower supports geometry (length of support, lt_s, diameter of support, d_{ts} and number of tower supports, n_{ts}) significantly influence the loss coefficient K_{ts}. From section 2 to 3, just before the entrance of heat exchanger bundles, air experiences losses due to heat exchanger supports, known as the heat exchanger support loss coefficient K_{hes}. While air stream flows to the inlet of heat exchanger bundles, there are changes in the fluid pattern and separation of air flow is observed which further adds the flow resistance known as the tower inlet loss coefficient, K_{ct}. From section 3 to 4, air experiences losses due to the contraction loss coefficient, K_{ctc}, the expansion loss coefficient, K_{cte} and the frictional loss coefficient K_{he}. Air properties change significantly at the discharge of the heat exchanger. From section 4 to 5, the air further losses its kinetic energy which is evaluated by the tower outlet loss coefficient, K_{to}. All these flow resistances are considered in calculating the draft equation which is essentially the pressure differential between inside and outside the tower.

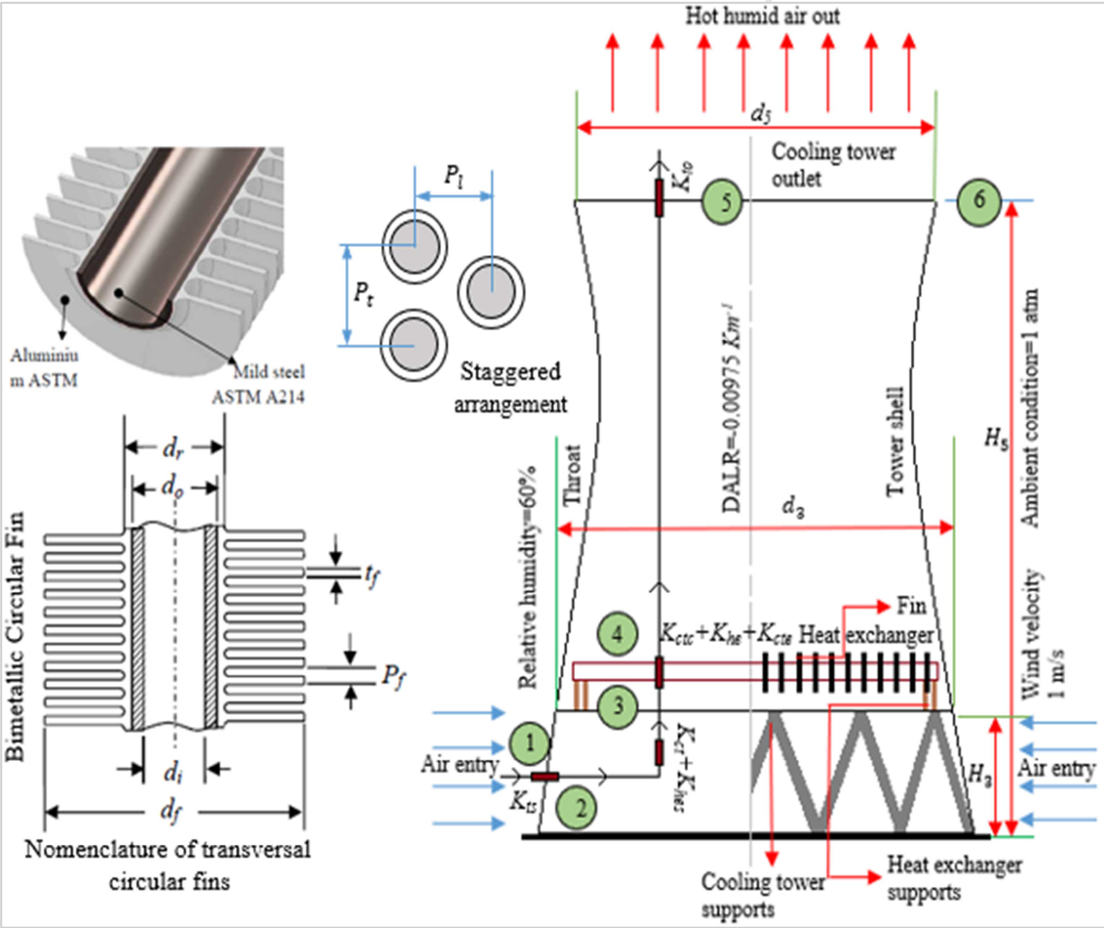

Fig. 4. Schematic diagram of NDDCT with finned tube heat exchanger bundles.

$$p_{a1} - \left[p_{a5} + \frac{\left(\frac{m_a}{A_5}\right)^2}{2\rho_{a5}} \right] = (K_{ts} + K_{ct} + K_{hes} + K_{ctc} + K_{he} + K_{cte}) \frac{\left(\frac{m_a}{A_{fr}}\right)^2}{2\rho_{a34}} + p_{a1}\left[1 - \left\{1 - 0.00975\frac{(H_3+H_4)}{2T_{a1}}\right\}^{3.5}\right] + p_{a4}\left[1 - \left\{1 - 0.00975\left(H_5 - \frac{H_3}{2} - \frac{H_4}{2}\right)T_{a4}\right\}^{3.5}\right] \quad (4)$$

The loss coefficients are shown with the following equations [36].

Tower support loss coefficient, $K_{ts} = \frac{2\Delta p_{ats}\rho_{a34}}{\left(\frac{m_a}{A_{fr}}\right)^2} = \frac{C_{Dts}L_{ts}d_{ts}n_{ts}A_{fr}^2}{(\pi d_3 H_3)^3}\left(\frac{\rho_{a34}}{\rho_{a1}}\right)$ (5)

Contraction coefficient, $K_{ctc} = (1 - \frac{2}{\sigma_c} + \frac{1}{\sigma_c^2})(\frac{\rho_{a34}}{\rho_{a1}})(\frac{A_{fr}}{A_{e3}})^2$ (6)

Expansion coefficient, $K_{cte} = (1 - \frac{A_{e3}}{A_3})^2(\frac{\rho_{a34}}{\rho_{a1}})(\frac{A_{fr}}{A_{e3}})^2$ (7)

Inlet loss coefficient, $K_{ct} = 0.072\left(\frac{d_3}{H_3}\right)^2 - 0.34\left(\frac{d_3}{H_3}\right) + 1.7$ (8)

Frictional loss coefficient, $K_{he} = 31383.9475Ry^{-0.332458} + \frac{2}{\sigma_a{}^2}(\frac{\rho_{a3}-\rho_{a4}}{\rho_{a3}+\rho_{a4}})$ (9)

Characteristic Reynolds number, $Ry = \frac{M_a}{\mu_{a34}A_{frT}}$ (10)

Outlet loss coefficient, $K_{to} = -0.28Fr_D^{-1} + 0.04Fr_D^{-1.5}$ (11)

Froude number, $Fr_D = \left(\frac{m_a}{A_5}\right)^2/[\rho_{a5}(\rho_{a6} - \rho_{a5})gd_5]$ (12)

The above equation is valid for $0.5 \le \frac{d_5}{d_3} \le 0.85$ and $5 \le K_{he} \le 40$

Table 3. Evaluation of pressure and temperature of the air at various states of the tower.

State point	Temperature	Pressure
1	$T_{a3} = 293\ K$	$p_{a1} = 1.01325x10^5$
2	$T_{a1} = T_{a2}$	$p_{a1} = p_{a2}$
3	$T_{a3} = T_{a1} - 0.00975H_3$	$p_{a6} = p_{a1}(1 - 0.00975\frac{H_3}{T_{a1}})^{3.5}$
4	T_{a4} =To be evaluated by the code	$p_{a4} = p_{a1}[1 - 0.00975\frac{(H_3+H_4)}{2T_{a1}}]^{3.5} - (K_{ts} + K_{ct} + K_{hes} + K_{ctc} + K_{he} + K_{cte})\frac{\left(\frac{M_a}{A_{fr}}\right)^2}{2\rho_{a34}}$
5	$T_{a5} = T_{a4} - 0.00975(H_5 - H_4)$	$p_{a5} = p_{a6} + \Delta p_{a56} = p_{a6} + K_{to}\frac{\left(\frac{M_a}{A_5}\right)^2}{2\rho_{a5}}$
6	$T_{a6} = T_{a1} - 0.00975H_6$	$p_{a6} = p_{a1}(1 - 0.00975\frac{H_5}{T_{a1}})^{3.5}$

Table. 4. Geometric details of heat exchanger unit.

Parameter	*Value*	*Parameter*	*Value*
Tube material	ASTM A214 mild steel	Fin type	Extruded bimetallic
Fin material	ASTM 6063 aluminium	Heat exchanger arrangement	horizontal
Fin Shape	Circular	Tube arrangement	staggered
Tube thermal conductivity, k_t	50 W/mK	Fin thermal conductivity, k_f	204 W/mK

Tube outside diameter, d_o	25.4 mm	Fin diameter, d_f	57.2 mm
Tube inside diameter, d_i	21.6 mm	Fin root diameter, d_r	27.6 mm
Relative tube surface roughness, ε/d_i	$5.24\text{x}10^{-4}$	Fin shape	Tapered
Tube rows, n_r	4	Fin tip thickness, t_{ft}	0.26 mm
No. of tubes per bundle, n_{tb}	154	Fin thickness (mean), t_f	0.48 mm
Tube pitch, P_t	58 mm	Fin root thickness, t_{fr}	0.74 mm
Tube pitch, P_l	50.22 mm	Fin Pitch, P_f	2.7 mm
Tube length, L_t	15 m	Air porosity, σ	0.433

In the present work, circular fins are employed on the tubes transversally to increase the heat transfer coefficient of the external fluid. The tubes are staggered to maximize heat exchange. The fins are of the bimetallic extruded type which are assumed to be perfectly bonded with no thermal contact resistance and made of mild steel. The variation of fin thermal conductivity k_t value of the fin is considered to be insignificant throughout the whole fin geometry. **Table 4**, demonstrates the geometric the details of air-cooled heat exchanger model adapted from ref. [36]. Cooling efficiency of the NDDCT is given by

$$\eta_C = \frac{Range}{Range+Approach} \tag{13}$$

Where, $Range = T_{si} - T_{cf}$ and $Approach = T_{si} - T_{wetb}$
Here T_{si}, T_{cf}, T_{wetb} are the cycle fluid inlet temperature, outlet temperature and air wet bulb temperature respectively.

4.2 Tower Modelling with MDK

The conventional log mean temperature difference (LMTD) method of modelling the heat exchanger is not adequate for precise calculation of heat transfer from sCO_2. The variation of thermodynamic and transport properties of sCO_2 with the change of temperature near the pseudocritical temperature is not accounted by the conventional method. Hence, the nodal method is applied while modelling the heat exchanger which takes into consideration of thermodynamic property changes for both tube side and air side. In this approach, a number of sub-heat exchangers are coupled serially and the traditional LMTD method is applied at each node to calculate the local properties. Using the nodal approach, the profile of local h_s of the cycle fluid with the change of temperature is obtained. **Fig. 5** demonstrates the flow procedure to model NDDCT.

MDK is a model development kit provided by IPSEpro used in the present work for detailed modelling of NDDCT in the power cycle. The IPSEpro does not contain a natural draft cooling tower model. Hence, MDK is used in the present work to investigate the cooling mechanism of sCO_2 by the air-cooled heat exchanger unit as well as to design the cooling tower to accomplish the duty requirements. The effect of different NDDCT design on the performance of the power plant is investigated. The model development language (MDL) is used for the mathematical model. The geometric parameters of NDDCT and the inlet condition of the cycle fluid and air are specified as inputs. The model starts computation with the preliminary estimates of the outlet temperatures and the number of bundles. The airside thermodynamic properties at various positions of the NDDCT are determined. For the tube side, REFPROP [41] is invoked by the program to calculate the sCO_2 thermodynamic properties at each node. The local bulk temperature, the corresponding heat transfer coefficient, and the local heat transfer are evaluated.

The air side characteristic Reynolds number and heat transfer coefficient are also evaluated. Next, the code calculates the tower geometry with the given inputs. The energy equations for both sides of the heat exchanger are concurrently solved. Various types of loss coefficients are determined to evaluate the draft equation and air mass flow rate inside NDDCT. If the design point sCO_2 outlet temperature is not reached, the code then changes the initial estimates and repeats the calculation. With a given input of a number of bundles, the code determines the tower geometry.

ACCEPTED MANUSCRIPT

ACCEPTED MANUSCRIPT

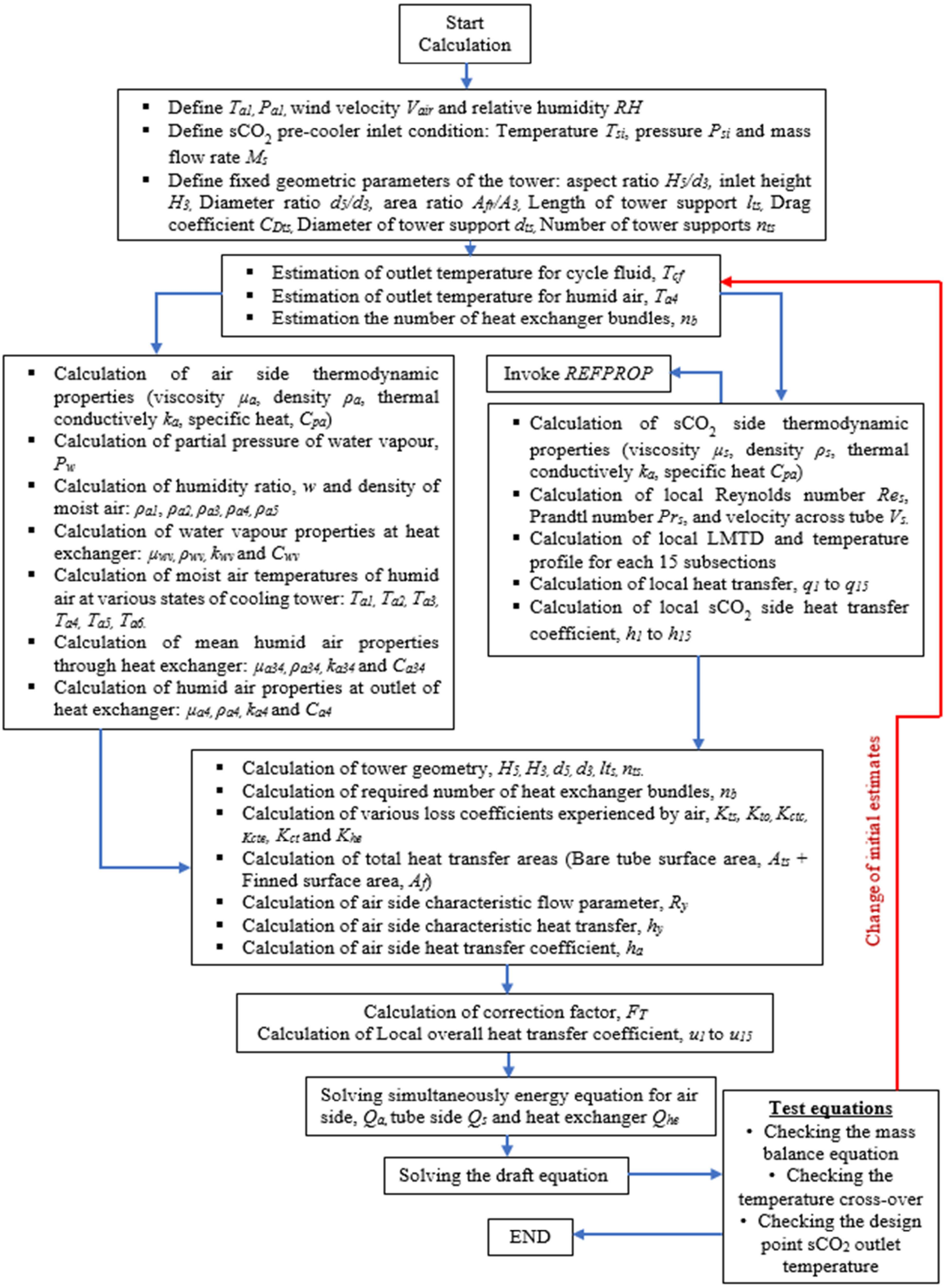

Fig. 5. Flow procedure applied in MDK to model NDDCT.

4.3 Optimum geometry of NDDCT

In order to determine the optimum geometry of the NDDCT, the influence of aspect ratio ($R_a=H_5/d_3$) and diameter ratio ($R_d=d_5/d_3$) on the tower performance is investigated. Increasing the aspect ratio increases the air mass flow per unit heat exchanger area. According to the study of [42], the optimum tower geometry depends on the tower elevation, H_5 with an optimum diameter ratio. In the present work, the aspect ratio is taken as 1.4. However, there is an optimum value of diameter ratio on the tower heat rejection and air mass flow rate, as shown in **Fig. 6**. Keeping the number of bundles, N_b fixed, the cycle fluid outlet temperature, T_{cf} shows insignificant change from R_d=0.7 onwards. At lower R_d, the cold flow incursion observed at the top of the tower adversely impacts on the cooling performance [43]. Hence, the convergent tower outlet is recommended to mitigate the influence of cold inflow. However, excessive restriction in tower outlet diameter increases the dynamic loss. Increasing the R_d also increases the tower cost linearly hence R_d=0.7 is taken as the optimum value. **Table 5**, shows the geometric inputs used in the present work to model the NDDCT.

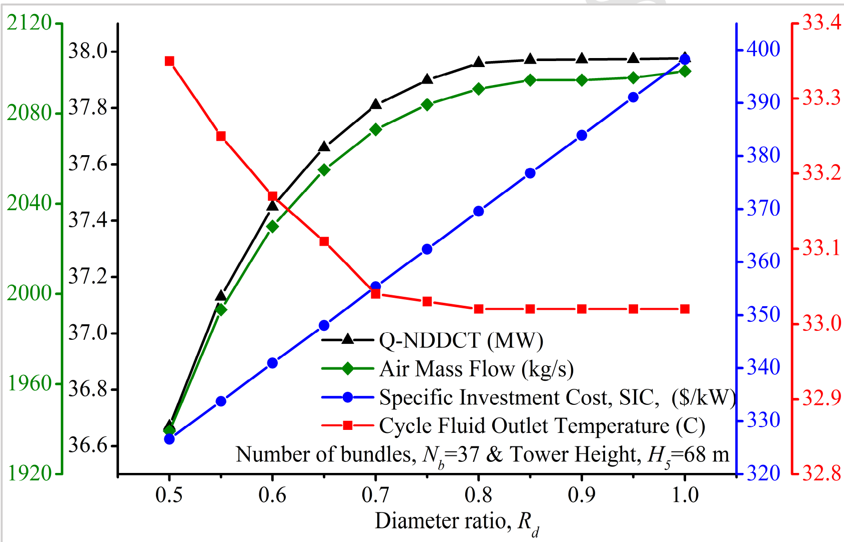

Fig. 6. Effect of diameter ratio on the various parameter of NDDCT.

Table. 5. Geometric details of NDDCT model.

Parameter	*Value*	*Parameter*	*Value*
Aspect ratio, R_a	1.4	Diameter ratio, R_d	0.7
Tower inlet height, H_3	(d_3/6.5) m	Length of tower support: *lts*	(H_3 x 1.15) m
Tower height, H_4	(H_3+H_{hx}) m	Support coefficient, C_{Dts}	2
Frontal area ratio, A_{frT}/A_3	0.65	Width of tower support, d_{ts}	0.4 m
		Number of tower supports: n_{ts}	d_3/1.38

4.4 Required Cooling System specification

Table 6, lists the calculated cooling system specifications at different plant capacities as the optimum values evaluated at the design condition. In all cases, the desired compressor inlet temperature of 33^{o}C is obtained that produces the highest η. As the plant capacity increases, the unit height heat rejection increases from 0.63 MW/m to 0.95 MW/m and the average Nusselt number increases from 1975 to 2168. **Fig. 7** shows how a selected number of parameters vary with the plant size. The cooling potential of the tower can also be determined by the amount of heat rejected by each heat exchanger bundle. For the 40 MW case, the average heat rejected by each bundle is 1.02 MW whereas for 100 MW the value is increased to 1.18 MW. It is obvious that the tower performance increases with higher capacity of a power plant in terms of the unit height heat rejection and the average heat rejected by each heat exchanger bundle. This figure also includes the specific investment cost, *SIC*, which decreases sharply with increasing capacity. The *SIC* is an economic parameter and the next section explains how it is determined.

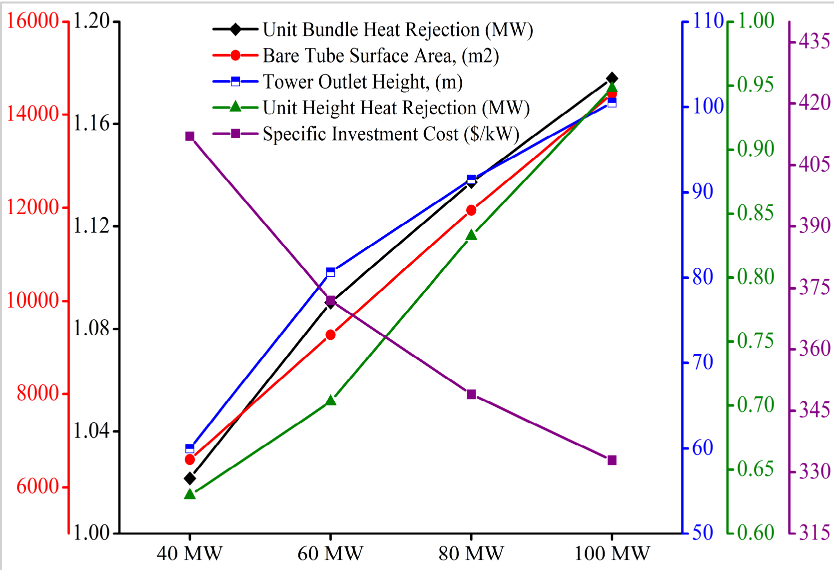

Fig. 7. Tower performance for various capacities of the power plant.

Table. 6. Optimized results of power cycle and NDDCT.

NDDCT				
Parameter	40 MW	60 MW	80 MW	100 MW
Heat Rejected, Q	37.8 MW	56.7 MW	76.2 MW	95.4 MW
Outlet height of the tower, H_5	68 m	80.64 m	91.53 m	100.65 m
% increase in tower height,	-	34.4 %	52.55 %	67.75 %
Unit height heat rejection	0.63 MW/m	0.7 MW/m	0.83 MW/m	0.95 MW/m
Heat Exchanger height from ground, H_4	7.7 m	9.09 m	10.3 m	11.3 m
Inlet height of the tower, H_3	7.47 m	8.86 m	10.06 m	11.06 m
Outlet tower diameter, d_5	34 m	40.32 m	45.76 m	50.32 m
Inlet tower diameter, d_3	48.48 m	57.6 m	65.38 m	71.88 m
Quantity of heat exchanger bundles, n_b	37	52	67	81
Average heat rejected by each bundle	1.02 MW	1.09 MW	1.14 MW	1.18 MW
Quantity of tower supports: n_{ts}	35	41	48	52
Tower support dimension: lts	8.62 m	10.23 m	11.61 m	12.77 m
Frontal area of heat exchanger bundles, A_{fr}	1205 m^2	1693 m^2	2183 m^2	2638 m^2
Air side surface area, A_a	0.886x10^6 m^2	1.25x10^{6}m^2	1.61x10^6 m^2	1.94x10^6 m^2
Tube side surface area, A_t	5567.83 m^2	7825.06 m^2	10082.3 m^2	12189 m^2
Bare tube side surface area, A_{tb}	6598.95 m^2	9274.2 m^2	11949.4 m^2	14446.3 m^2
% increase in surface area	-	40.54 %	81.09 %	118.91 %
Correction factor, F_T	0.945	0.947	0.949	0.950
Overall thermal conductance, UA	3775.68 kW/K	5549.9kW/K	7384.8kW/K	9155.63kW/K
Characteristic Reynolds number, R_y	97700.4 m^{-1}	106766 m^{-1}	113798 m^{-1}	119496 m^{-1}
Average Nusselt Number, Nu	1975.72	2069.59	2117.97	2168.17
sCO_2 inlet velocity, v_s	0.76 m/s	0.82 m/s	0.84 m/s	0.86 m/s
sCO_2 mean outlet temperature, T_{cf}	33^{o}C	33^{o}C	33^{o}C	33^{o}C

ACCEPTED MANUSCRIPT

Power Cycle				
Parameter	40 MW	60 MW	80 MW	100 MW
Heat input in PHE	48.7 MW	78 MW	156.1 MW	195.1 MW
Turbine Work	33.1 MW	53 MW	106.1 MW	132.7 MW
RC compression work	5.1 MW	8.3 MW	16.5 MW	20.6 MW
MC compression work	3 MW	4.8 MW	9.6 MW	12.1 MW
Heat recuperated in HTR	104.4 MW	168.7 MW	337.4 MW	421.8 MW
Heat recuperated in LTR	28.6 MW	45.8 MW	91.6 MW	114.6 MW
sCO_2 mass flow	388 Kg/s	583 Kg/s	778 Kg/s	972 Kg/s

4.5 Economic Analysis of NDDCT

Table 7 demonstrates the detailed cost model of the NDDCT adapted from ref [42, 44, 45]. **Table 8**, shows the cost comparison for various capacities of NDDCT. The cost model includes capital cost, labour cost, maintenance cost, annual operating cost, and specific investment cost. As shown before, tower performance improves with plant capacity. The *SIC* also decreases from 412 $/kW to 333 $/kW when the size is increased from 40 to 100 MW. For instance, to build the cooling tower for the 80MW solar thermal power plant, it is beneficial from an economic perspective to construct one tower instead of two short towers of each 40 MW capacity. One big tower is recommended over multiple short towers for a power plant with the higher thermal output.

Table 7. Cost equations for heat exchanger and NDDCT.

Cost of Heat Exchanger	
Parameter	*Equation*
Fin cost per unit tube length, C_f	$C_f = \frac{\pi(d_f^2 - d_r^2)}{4} t_f \left(\frac{1}{P_f + t_f} + 1\right) \rho_{al} C_{ual} + C_{af}$ ρ_{al} is the density of fin material made of aluminum, C_{ual} is the unit cost of aluminum taken as 6 $/kg and C_{af} is the fabrication cost taken as 0.4 $/kg.
Tube cost per unit tube length, C_t	$C_t = \frac{\pi[d_r^2 - (d_r - 2\epsilon_t)^2]}{4} \rho_{steel} C_{ut} + C_{at}$ ρ_{steel} is the density of tube material made of steel, C_{ut} is the unit cost of steel taken as 1.6 $/kg and C_{at} is the fabrication cost taken as 4 $/kg.
Total finned tube cost, C_{ft}	$C_{ft} = n_b n_t n_r L_t (C_f + C_t)$ L_t is the length of heat exchanger bundle.
Heat exchanger header cost, C_{header}	$C_{header} = C_{ft} f_{header}$ f_{header} is the weighting factor taken as 0.2.
Heat exchanger labour cost, C_{labour}	$C_{labour} = (C_{ft} + C_{header}) f_{labour}$ f_{labour} is the labour cost weighting factor taken as 0.8.
Total cost of heat exchanger, C_{he}	$C_{he} = (C_{ft} + C_{header} + C_{labour}) f_{he}$ f_{he} is the heat exchanger weighting factor taken as 1.2.
Cost of NDDCT	
Parameter	*Equation*
Tower shell cost, C_{shell}	$C_{shell} = \frac{2.4(D_3 + D_5)}{H_5}(1392.2H_5^2 - 31937H_5 + 10^6)$
Foundation cost, $C_{foundation}$	$C_{foundation} = f_{foundation} D_3$ $f_{foundation}$ is the unit cost of tower foundation taken as 22,372 $/m.
Tower support cost, $C_{support}$	$C_{support} = C_{foundation} f_{support}$ $f_{support}$ is the weighting factor of support taken as 0.6
Tower labour cost, $C_{tlabour}$	$C_{tlabour} = \left(C_{shell} + C_{support} + C_{foundation}\right) f_{tlabour}$ $f_{tlabour}$ is the weighting factor for labour taken as 1.0.
Total NDDCT cost, C_{tower}	$C_{tower} = (C_{shell} + C_{support} + C_{foundation} + C_{tlabour}) f_{tower}$

ACCEPTED MANUSCRIPT

ACCEPTED MANUSCRIPT

	f_{tower} is the weighting factor for tower taken as 1.2.
Maintenance and Annual Cost	
Parameter	*Equation*
Maintenance cost, C_{MC} Fixed charged rate, K Annual cost, C_{annual} Specific investment cost, *SIC*	$C_{MC} = 0.01C_{he} + 0.005C_{tower}$ $K = \frac{i(1+i)^n}{(1+i)^n - 1}$ i is the interest rate of 9% and n is the repayment period of 30 years. $C_{annual} = K(C_{he} + C_{tower}) + C_{MC}$ $SIC = \frac{(C_{he}+C_{tower})\eta}{W_{net}(1-\eta)}$ in \$/kW

Table 8. NDDCT Cost comparison in AUD $ for various capacities of the power plant.

Parameter	40 MW	60 MW	80 MW	100 MW
Total cost of the heat exchanger, C_{he}	2,212,184	3,109,016	4,005,847	4,842,890
Tower labour cost, $C_{tlabour}$	5,567,626	7,509,923	9,436,564	11,223,096
Total NDDCT cost, C_{tower}	13,362,304	18,023,816	22,647,754	29,635,430
Maintenance cost, C_{MC}	28,802	40,102	51,382	61,896
Annual cost, C_{annual}	1,544,766	2,097,094	2,645,746	3,155,082
Specific investment cost, *SIC*	412 ($/kW)	372 ($/kW)	349 ($/kW)	333 ($/kW)

5. Results and Discussion

5.1 Tower sizing

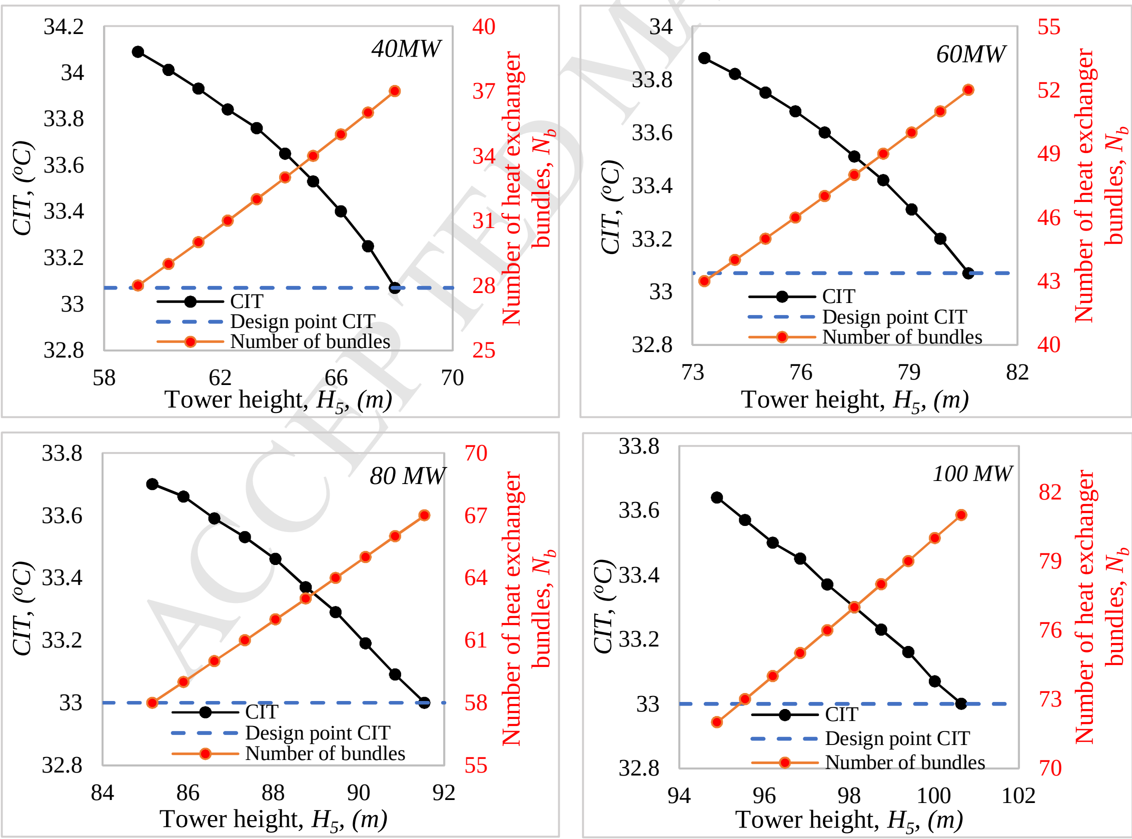

Fig. 8. Variation of CIT with tower height.

Fig. 8 show the variation of compressor inlet temperature and the required number of air-cooled heat exchanger bundles with the tower outlet height for 40 MW, 60 MW, 80 MW, and 100 MW respectively. As the tower height gradually increases, this causes the reduction of the cycle fluid outlet temperature. Since 33°C is the optimum compressor inlet temperature in the prescribed operating condition, the NDDCT is designed according to this design point. The N_b also increases proportionately with the increase of tower height.

5.2 Heat Transfer Characteristics

Fig. 9(a) shows the variation of the tube-side heat transfer coefficient h_s and local tube side velocity profile for various power plants. The h_s value sharply increases around tube length position of x/L=0.7 when the temperature is near pseudocritical temperature, T_{pc} (T_{pc}=34.3°C). When the bulk temperature is below the T_{pc}, the h_s value sharply falls for the rest of the tube length. Since the Reynolds number is higher at higher power plant capacities, higher h_s are attained for 60 MW, 80 MW, and 100 MW cases. At the inlet of the tube, the tube velocity is significantly higher since the density of the gas is significantly lower. As the temperature of the T_s gradually decreases, the fluid density and the viscosity both increase which decrease the Re along the length of the tube. The tube velocity is higher for 60 MW, 80 MW, and 100 MW cases.

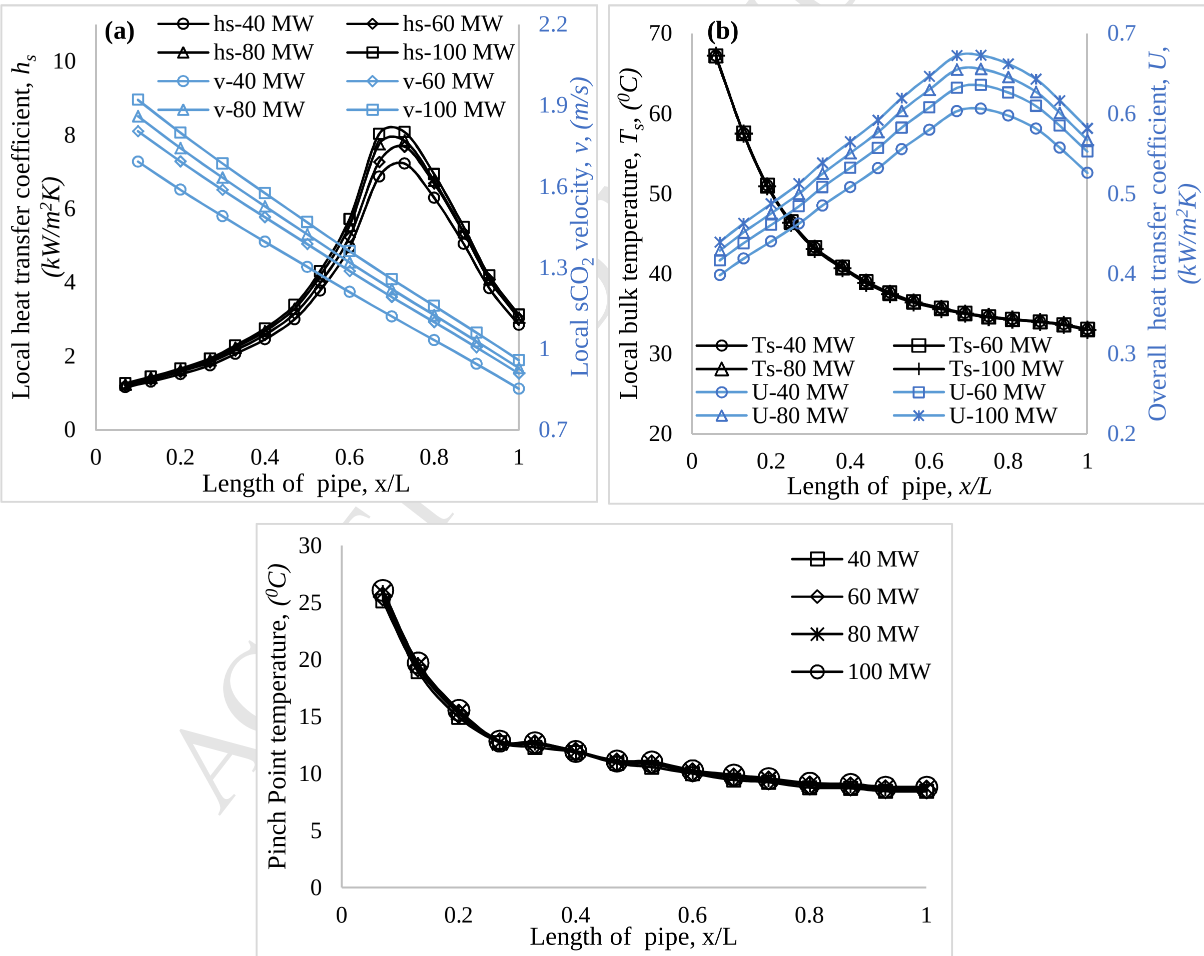

Fig. 9. (a) Local fluid velocity and h_s profile, (b) U and T_s profile for various capacities of power, (c) variation of pinch point temperature along the length.

Fig. 9(b) reveals the lengthwise T_s and U profiles of the cycle fluid. For all cases, the desired sCO_2 outlet temperature is reached. From tube position x/L=0.7 onwards, the trend of T_s profile becomes flat due to the sharp rise of isobaric specific heat in the vicinity of the pseudocritical region. Similarly, the profile of the overall heat transfer coefficient, U is also shown by considering the air side heat transfer coefficient. Likewise, the h_s, the U shows similar trend along the tube length. **Fig. 9 (c)** demonstrates the pinch point temperature along the length for all four cases. No pinch point violation occurs in any parts of the air-cooled heat exchanger. During each iteration, our model checks any temperature cross-over (pinch point degradation) in any parts of the heat exchangers. The simulation result confirms no violation of pinch point constraint in the heat exchangers and NDDCT.

5.3 Evaluation of loss coefficients

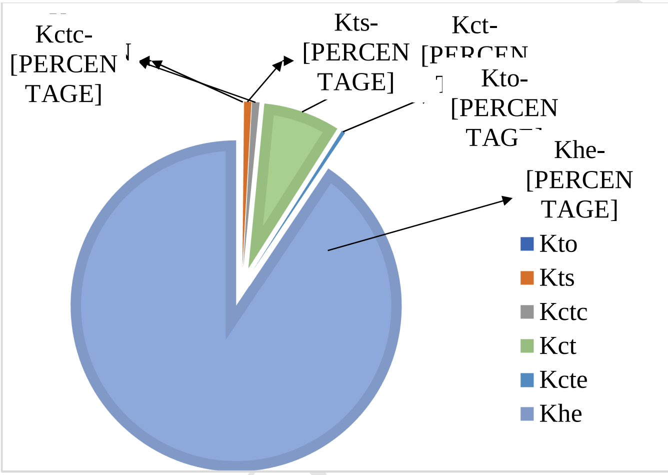

Fig. 10. Proportions of different loss coefficients for 40 MW NDDCT.

Fig. 10 demonstrates the proportion of various loss coefficients due to the flow resistances at the various position of cooling tower for the 40 MW case. The heat exchanger loss coefficient, K_{he} contributes the majority of the losses (about 91%) due to the fluid friction in the heat exchanger tube bundles. Next, the K_{ct} contributes about 7% of the total loss due to the fact of distorted air velocity profile before the entrance of heat exchanger bundles and separation of flow at the inlet of the NDDCT. The other loss coefficients $K_{ctc,}$ $K_{cte,}$ $K_{to,}$ and K_{ts} are comparatively lower in comparison with the K_{he} and K_{ct}. All these flow resistances are taken into consideration while evaluating the draft equation of the NDDCT.

In the next section, the thermal assessment of the power plant integrated with the detailed NDDCT model is demonstrated by investigating the η, the exergy efficiency and the cooling efficiency of the NDDCT. The results are only shown for 40 MW case since similar performance is observed for other power plants with an output of 60 MW, 80 MW, and 100 MW.

5.4 Influence of NDDCT inlet temperature

The effect of NDDCT inlet temperature on the η and the split ratio is shown in **Fig. 11(a)**. Increasing the sCO_2 temperature from 65^{0}C to 110^{0}C, the η significantly drops from 52.2% to 42.6%. The split ratio decreases up to 75^{0}C and then increases exponentially to 62.7%. **Fig. 11(b)** reveals the variation of heat transfer in the heat exchangers and NDDCT with the increase of NDDCT inlet temperature. The heat transfer in the HTR decreases from 169.2 MW to 135.5

MW, and for LTR, the value increases from 45.6 MW to 68.8 MW. The heat addition to the primary heat exchanger increases (78 MW to 96 MW) with inlet temperature which also reduces the η. Higher inlet temperature also augments the initial temperature differential of the fluid streams inside the NDDCT for which the heat dumped by the NDDCT rises from 38.1 MW to 56.5 MW.

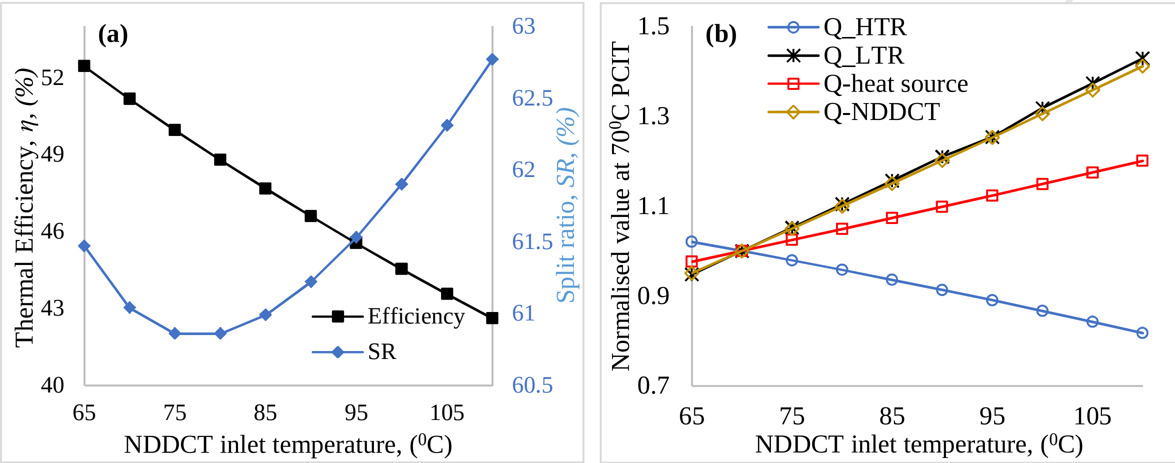

Fig. 11. (a) Effect of NDDCT inlet temperature on η and *SR* and (b) heat transfer rate in the heat exchangers and NDDCT.

5.5 Impact of Air Temperature

The impact of air temperature on the net power generation and total compression work is shown in **Fig. 12**. The cycle performance is reduced from 40 MW to 31.9 MW when the temperature rises from 20°C to 50⁰C. The total compression work increases from 12.1 MW to 21.2 MW with air temperature. The MC compression work considerably increases with air temperature. Increasing the air temperature decreases the air mass flow inside the NDDCT and increases cycle mass flow into the NDDCT. The air mass flow almost linearly decreases from 2072 Kg/s to 1737 Kg/s. The variation of cycle mass flow is due to the change in *SR* with air temperature.

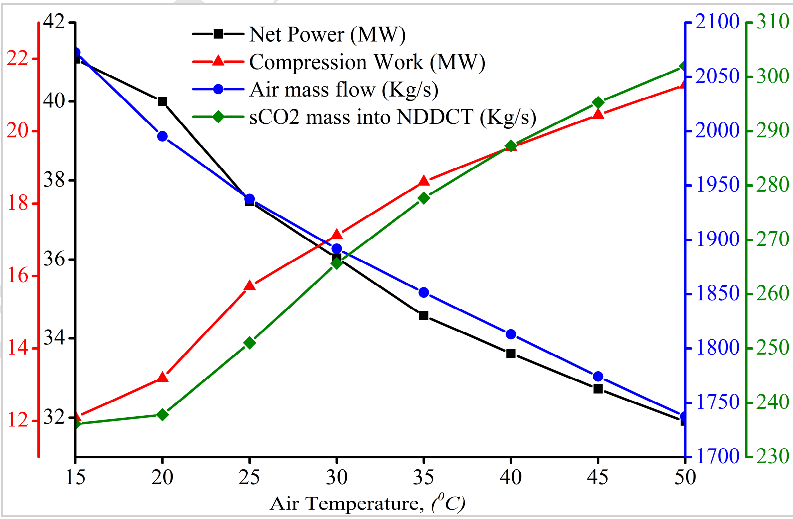

Fig. 12. Influence of air temperature on cycle performance, cycle mass flow and air mass flow.

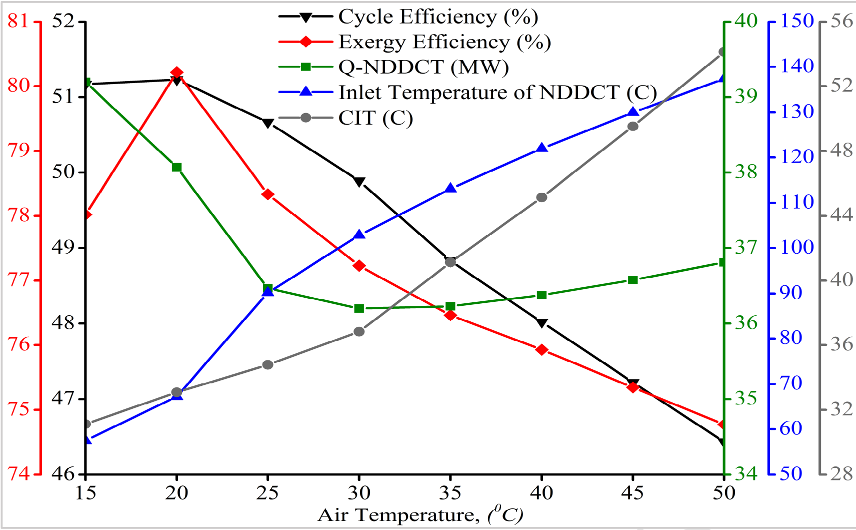

Fig. 13. The change of exergy efficiency, cycle efficiency, and other parameters with ambient air.

The change of inlet and outlet temperatures of sCO_2 inside NDDCT is shown in **Fig. 13**. As the air temperature rises, the inlet temperature of the cycle fluid in NDDCT also increases. The compressor inlet temperature increases almost linearly. The heat rejection in the NDDCT depends on the sCO_2 and air temperatures and first sharply decreases up to 30^0C air temperature and then insignificantly increases at higher air temperatures. The η and the η_E both decrease with air temperature and both parameters are maximum at the design point temperature of 20^0C. The η_E decreases from 80.2% to 74.7%. These results show that the net power output from an air-cooled sCO_2 power generator deviates significantly from its design-point output when the air temperature differs from the design-point air temperature value. This means that the selection of the design-point air temperature is one of the important design choices when designing a sCO_2 power generator.

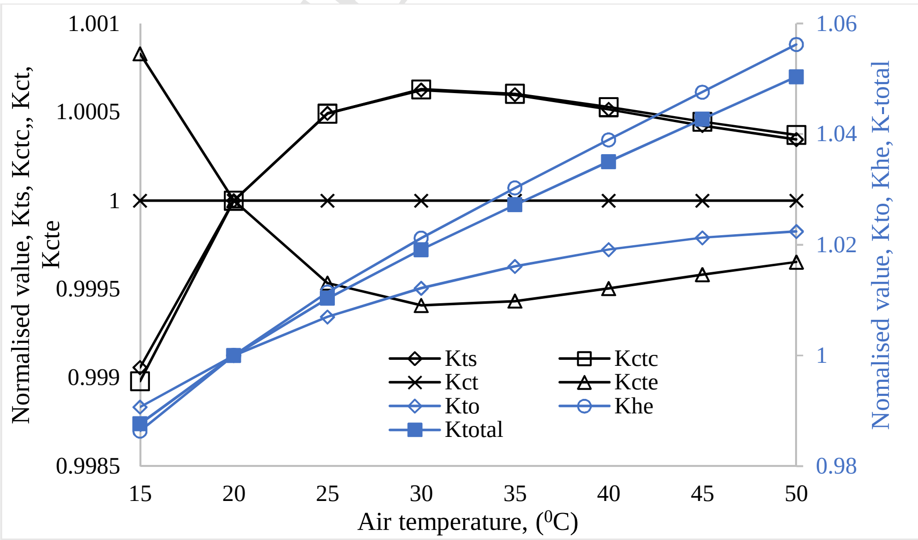

Fig. 14. Normalized values of loss coefficients at various ambient temperature.

The contribution of various loss coefficients experienced by air inside the NDDCT at various air temperature is shown in **Fig. 14**. The K_{ctc} and K_{ts} both increases up to air temperature of 30^0C and then monotonously decreases with air temperature. The K_{ct} remains constant with the air temperature since the value of K_{ct} is independent of fluid properties and determined from the given geometry of the tower. The K_{to} and K_{he} both increase with air temperature. The overall effect is the increase of total loss coefficient, K_{total} with the air temperature.

5.6 Cooling Potential of NDDCT

The cooling potential of the NDDCT can be determined from the evaluation of cooling efficiency. The range of the tower increases with air temperature due to the increase in both inlet and outlet temperature of sCO_2 in NDDCT, as shown in **Fig. 15**. The tower approach decreases and the cooling efficiency increases with air temperature. However, this improvement of cooling efficiency is not beneficial for the power plant since the cycle η significantly drops with air temperature.

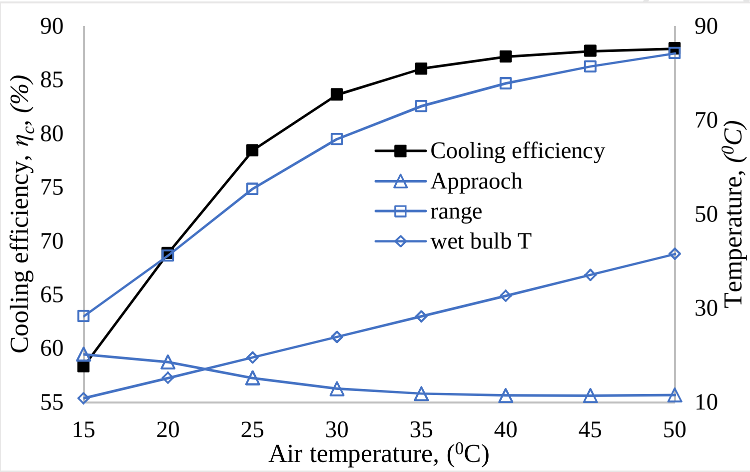

Fig. 15. The range, approach and cooling efficiency at various air temperature.

5.7 Irreversibility Analysis

The component wise irreversibility contribution at 20^{0}C air temperature is depicted in **Fig. 16**. The heat source heat exchanger contributes the highest irreversibility of 68.75 MW. The HTR, NDDCT, and Turbine contribute 21%, 15% and 13% of the total irreversibility. The equations to evaluate the irreversibility in the present work is shown in **Table 9**. The variation of component-wise irreversibility with air temperature is shown in **Fig. 17**. In NDDCT, increasing the air temperature significantly increases exergy input due to an increase of sCO_2 inlet temperature. The energy gained by ambient air shows no significant change. The overall impact, the I_{NDDCT} increases from 2.6 MW to 3.7 MW. In the primary heat exchanger, the exergy input decreases for the acquirement of the same outlet temperature for which the I_{PHE} decreases from 6.1 MW to 5.4 MW with ambient air. The irreversibility of the RC compressor shows little variation with air temperature and I_{MC} and $I_{Turbine}$ both increase with air temperature. The I_{HTR} shows its maximum value of 4.8 MW at 15^{0}C air temperature and then significantly drops to 1.7 MW at 50^{0}C air temperature. The highest irreversibility of 6.1 MW is found from the primary heat exchanger at 15^{0}C air temperature. The total irreversibility of the power cycle decreases from 17.2 MW to 15.5 MW with an increase in air temperature. Increasing the air temperature gradually rises the sCO_2 inlet temperature of the heat source from 484^{0}C to 508^{0}C. The reduction of total irreversibility is due to the requirement of lesser exergy input from the primary heat exchanger at higher air temperature.

ACCEPTED MANUSCRIPT

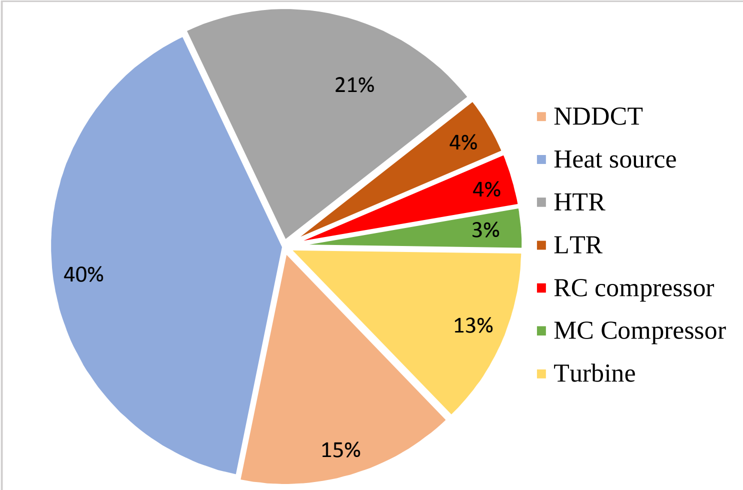

Fig. 16. The component wise irreversibility contribution at 20^{0}C air temperature.

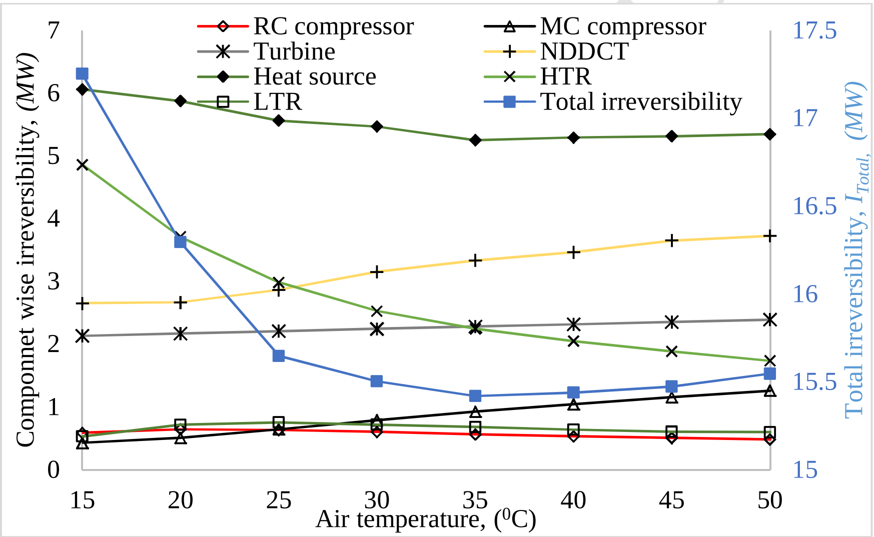

Fig. 17. Irreversibility variation with air temperature.

Table 9. Irreversibility equations for individual components.

Component	Equation
Primary Heat Exchanger	$I_{PHE} = [m_c(h_{in} - h_{out}) - T_0(s_{in} - s_{out})] - [m_s(h_4 - h_5) - T_0(s_4 - s_5)]$
High-temperature recuperator	$I_{HTR} = [m_s(h_6 - h_7) - T_0(s_6 - s_7)] - [m_s(h_4 - h_3) - T_0(s_4 - s_3)]$
Low-Temperature recuperator	$I_{LTR} = [m_s(h_7 - h_8) - T_0(s_7 - s_8)] - X[m_s(h_2 - h_3) - T_0(s_2 - s_3)]$
NDDCT	$I_{NDDCT} = (1 - X)[m_s(h_8 - h_1) - T_0(s_8 - s_1)] - [m_a(h_0 - h_i) - T_0(s_o - s_i)]$
RC compressor	$I_{RC} = (1 - X)W_{RC} - (1 - X)[m_s(h_3 - h_8) - T_0(s_3 - s_8)]$
MC compressor	$I_{MC} = XW_{MC} - X[m_s(h_2 - h_1) - T_0(s_2 - s_1)]$
Turbine	$I_{Turbine} = m_s(h_5 - h_6) - T_0(s_5 - s_6)] - W_T$

ACCEPTED MANUSCRIPT

5.8 Comparison Against Wet Cooling System

In general, power cycles in CSP application are mostly located in a hot climate where solar insolation is quite high. However, the abundant fresh water supply to cool the working fluid is indeed a great challenge. In comparison with the traditional steam cycle, the sCO_2 power cycle is mostly suited with the dry cooling system in terms of lower requirement of air mass flow rate, lower parasitic losses, lower thermal irreversibilities, and smoother cooling profile of sCO_2 and air. The dry cooled steam cycle efficiency significantly drops at higher ambient temperature. However, this not the case for dry cooled sCO_2 power cycle, since the efficiency is significantly higher during hot climate. Hence, dry cooling is treated as an alternative to a wet cooling system for sCO_2 power cycles in the CSP application. Although the wet coolers are more efficient than the dry cooling system, the choice of wet coolers in CSP is eliminated in the present work due to the inaccessibility of water. There are environmental issues with wet coolers such as water evaporation, accumulation of dissolved solids, and corrosion. In comparison with the traditional steam cycle, this sCO_2 power cycle can still provide higher thermal efficiency even with dry cooling [4, 21]. The acquirement of higher efficiency with dry cooled sCO_2 power cycles allows the potential applicability of dry cooling in CSP application. Compared to the forced draft system, the NDDCT offers no parasitic losses. At higher ambient condition, there is an efficiency penalty with dry cooling. To compensate for this performance degradation, various cooling techniques can be applied. Zeyghami and Khalili [30] proposed a radiative cooling system incorporated as an additional cooling component of an air cooling system to enhance the cooling performance of the power cycle by cooling it to the desired temperature. Another remedy would be the hybrid cooling approach. Several studies (Sadafi et al. [46, 47], Alkhedhair et al. [48], Zou et al. [35] are available in the literature to compensate the performance degradation with the dry cooling system.

5.9 Design Recommendation of NDDCT

The present work emphasizes the design methodology of the dry cooling system applicable to a sCO_2 power cycle. Before designing the NDDCT, the optimum operating condition of the power cycle needs to be rectified based on the prescribed boundary condition. For a specific CSP location, the design parameter (air temperature and solar irradiation) of the tower is of great importance. The present analysis does not refer to any specific location, however, it provides a comprehensive guideline in designing the cooling tower and it is still applicable for higher air temperature values. Various geometric inputs of the tower (aspect ratio, diameter ratio, and frontal area ratio) must be optimized before conducting the economic analysis.

Conclusion

The thermal performance of the power plant is investigated by demonstrating the η, the η_E, the cooling efficiency, and the irreversibility analysis. The major findings of the analysis are summarised below.

- In the preliminary analysis, the effect of the pressure ratio on the W_{net}, the η, and the SR is investigated. The η is maximum at the lowest SR. The η also increases when the main compressor inlet temperature increases in the range of 30^0C to 33^0C. This suggests a unique heat transfer of sCO_2 due to a sharp change in transport properties near the pseudocritical temperature.

- Various geometric parameters are optimized prior to the design of the cooling tower. Next, the NDDCT is designed for various capacities of the power plant. The tower performance is evaluated in terms of unit height heat rejection and average heat rejection by each bundle. The higher the tower, the better the tower thermal performance. Detailed economic analysis of NDDCT is performed based on optimized geometry.
- The variation of NDDCT inlet temperature on the cycle performance is also investigated. Both the η and W_{net} significantly decrease with the increase of NDDCT inlet temperature. The increase in air temperature causes the increase of the main compressor inlet temperature considerably which finally reduces the cycle performance.
- The irreversibility analysis shows that the primary heat exchanger, the HTR, and the NDDCT contribute the major portions of the total irreversibility. The physical reasoning of the change of irreversibility with air temperature is also explained. The total irreversibility reduces with the increase in air temperature.
- The advantages of dry-cooled sCO_2 power cycles are discussed compared to steam Rankine cycle. The possible remedies to compensate for the performance degradation with dry cooling during higher ambient temperature are also briefly discussed. The design recommendation of NDDCT is explained.

ACKNOWLEDGEMENT

The first author thanks the University of Queensland for granting Research Training Program (RTP) scholarship. The authors thank the Henan Centre for outstanding oversea scientists' support. This research was performed as part of the Australia Solar Thermal Research Initiative (ASTRI), a project supported by the Australia Government, through the Australia Renewable Energy Agency (ARENA).

REFERENCES

[1] C. S. Turchi, Z. Ma, T. W. Neises, and M. J. Wagner, "Thermodynamic study of advanced supercritical carbon dioxide power cycles for concentrating solar power systems," *Journal of Solar Energy Engineering,* vol. 135, no. 4, p. 041007, 2013.

[2] V. Dostal, P. Hejzlar, and M. J. Driscoll, "High-performance supercritical carbon dioxide cycle for next-generation nuclear reactors," *Nuclear Technology,* vol. 154, no. 3, pp. 265-282, 2006.

[3] T. Neises and C. Turchi, "A comparison of supercritical carbon dioxide power cycle configurations with an emphasis on CSP applications," *Energy Procedia,* vol. 49, pp. 1187-1196, 2014.

[4] Z. Ma and C. S. Turchi, "Advanced Supercritical Carbon Dioxide Power Cycle Configurations for Use in Concentrating Solar Power Systems: Preprint," National Renewable Energy Laboratory (NREL), Golden, CO.2011.

[5] L. Cheng, "Evaluation of Correlations for Supercritical CO2 Cooling Convective Heat Transfer and Pressure Drop in Macro-and Micro-Scale Tubes," *International Journal of Microscale and Nanoscale Thermal and Fluid Transport Phenomena,* vol. 5, no. 2, p. 113, 2014.

[6] B. D. Iverson, T. M. Conboy, J. J. Pasch, and A. M. Kruizenga, "Supercritical CO2 Brayton cycles for solar-thermal energy," *Applied Energy,* vol. 111, pp. 957-970, 2013.

[7] M. Persichilli, A. Kacludis, E. Zdankiewicz, and T. Held, "Supercritical CO2 power cycle developments and commercialization: why sCO2 can displace steam ste," *Power-Gen India & Central Asia,* 2012.

[8] K. J. Kimball and E. M. Clementoni, "Supercritical carbon dioxide brayton power cycle development overview," in *ASME Turbo Expo 2012: Turbine Technical Conference and Exposition*, 2012, pp. 931-940: American Society of Mechanical Engineers.

[9] P. Garg, P. Kumar, and K. Srinivasan, "Supercritical carbon dioxide Brayton cycle for concentrated solar power," *The Journal of Supercritical Fluids,* vol. 76, pp. 54-60, 2013.

ACCEPTED MANUSCRIPT

[10] T. Conboy, S. Wright, J. Pasch, D. Fleming, G. Rochau, and R. Fuller, "Performance characteristics of an operating supercritical CO2 Brayton cycle," *Journal of Engineering for Gas Turbines and Power,* vol. 134, no. 11, p. 111703, 2012.

[11] M. M. Ehsan, Z. Guan, and A. Klimenko, "A comprehensive review on heat transfer and pressure drop characteristics and correlations with supercritical CO 2 under heating and cooling applications," *Renewable and Sustainable Energy Reviews,* vol. 92, pp. 658-675, 2018.

[12] J. Xu, E. Sun, M. Li, H. Liu, and B. Zhu, "Key issues and solution strategies for supercritical carbon dioxide coal fired power plant," *Energy,* vol. 157, pp. 227-246, 2018.

[13] F. A. Al-Sulaiman and M. Atif, "Performance comparison of different supercritical carbon dioxide Brayton cycles integrated with a solar power tower," *Energy,* vol. 82, pp. 61-71, 2015.

[14] Y. Ma, X. Zhang, M. Liu, J. Yan, and J. Liu, "Proposal and assessment of a novel supercritical CO2 Brayton cycle integrated with LiBr absorption chiller for concentrated solar power applications," *Energy,* vol. 148, pp. 839-854, 2018.

[15] H.-H. Zhu, K. Wang, and Y.-L. He, "Thermodynamic analysis and comparison for different direct-heated supercritical CO2 Brayton cycles integrated into a solar thermal power tower system," *Energy,* vol. 140, pp. 144-157, 2017.

[16] K. Wang and Y.-L. He, "Thermodynamic analysis and optimization of a molten salt solar power tower integrated with a recompression supercritical CO2 Brayton cycle based on integrated modeling," *Energy Conversion and Management,* vol. 135, pp. 336-350, 2017.

[17] K. Wang, Y.-L. He, and H.-H. Zhu, "Integration between supercritical CO2 Brayton cycles and molten salt solar power towers: A review and a comprehensive comparison of different cycle layouts," *Applied energy,* vol. 195, pp. 819-836, 2017.

[18] M. Binotti, M. Astolfi, S. Campanari, G. Manzolini, and P. Silva, "Preliminary assessment of sCO2 cycles for power generation in CSP solar tower plants," *Applied Energy,* vol. 204, pp. 1007-1017, 2017.

[19] D. Milani, M. T. Luu, R. McNaughton, and A. Abbas, "A comparative study of solar heliostat assisted supercritical CO2 recompression Brayton cycles: dynamic modelling and control strategies," *The Journal of Supercritical Fluids,* vol. 120, pp. 113-124, 2017.

[20] D. Milani, M. T. Luu, R. McNaughton, and A. Abbas, "Optimizing an advanced hybrid of solar-assisted supercritical CO2 Brayton cycle: A vital transition for low-carbon power generation industry," *Energy Conversion and Management,* vol. 148, pp. 1317-1331, 2017.

[21] T. Conboy, M. Carlson, and G. Rochau, "Dry-Cooled Supercritical CO2 Power for Advanced Nuclear Reactors," *Journal of Engineering for Gas Turbines and Power,* vol. 137, no. 1, p. 012901, 2015.

[22] J. Dyreby, S. Klein, G. Nellis, and D. Reindl, "Design considerations for supercritical carbon dioxide Brayton cycles with recompression," *Journal of Engineering for Gas Turbines and Power,* vol. 136, no. 10, p. 101701, 2014.

[23] R. V. Padilla, Y. C. S. Too, R. Benito, and W. Stein, "Exergetic analysis of supercritical CO 2 Brayton cycles integrated with solar central receivers," *Applied Energy,* vol. 148, pp. 348-365, 2015.

[24] R. V. Padilla, R. Benito, and W. Stein, "An exergy analysis of recompression supercritical CO2 cycles with and without reheating," *Energy Procedia,* vol. 69, pp. 1181-1191, 2015.

[25] A. Moisseytsev and J. J. Sienicki, "Investigation of a dry air cooling option for an S-CO2 cycle," in *Supercritical CO2 Power Symposium, Pittsburgh (PA), Sep 9e10*, 2014.

[26] C. K. Ho, M. Carlson, P. Garg, and P. Kumar, "Technoeconomic analysis of alternative solarized s-CO2 Brayton cycle configurations," *Journal of Solar Energy Engineering,* vol. 138, no. 5, p. 051008, 2016.

[27] F. G. Battisti, J. M. Cardemil, and A. K. da Silva, "A multivariable optimization of a Brayton power cycle operating with CO2 as working fluid," *Energy,* vol. 112, pp. 908-916, 2016.

[28] M. T. Luu, D. Milani, R. McNaughton, and A. Abbas, "Dynamic modelling and start-up operation of a solar-assisted recompression supercritical CO2 Brayton power cycle," *Applied Energy,* vol. 199, pp. 247-263, 2017.

[29] S. Son and J. I. Lee, "Application of adjoint sensitivity analysis method to supercritical CO 2 power cycle optimization," *Energy,* vol. 147, pp. 1153-1164, 2018.

[30] M. Zeyghami and F. Khalili, "Performance improvement of dry cooled advanced concentrating solar power plants using daytime radiative cooling," *Energy Conversion and Management,* vol. 106, pp. 10-20, 2015.

[31] S. Duniam, I. Jahn, K. Hooman, Y. Lu, and A. Veeraragavan, "Comparison of direct and indirect natural draft dry cooling tower cooling of the sCO2 Brayton cycle for concentrated solar power plants," *Applied Thermal Engineering,* vol. 130, pp. 1070-1080, 2018.

ACCEPTED MANUSCRIPT

ACCEPTED MANUSCRIPT

[32] M. M. Ehsan, Z. Guan, A. Klimenko, and X. Wang, "Design and comparison of direct and indirect cooling system for 25 MW solar power plant operated with supercritical CO 2 cycle," *Energy Conversion and Management,* vol. 168, pp. 611-628, 2018.

[33] M. M. Ehsan, X. Wang, Z. Guan, and A. Klimenko, "Design and performance study of dry cooling system for 25 MW solar power plant operated with supercritical CO 2 cycle," *International Journal of Thermal Sciences,* vol. 132, pp. 398-410, 2018.

[34] Z. Guan, K. Hooman, and H. Gurgenci, "Dry cooling towers for geothermal power plants," *Alternative Energy and Shale Gas Encyclopedia,* pp. 333-349, 2016.

[35] Z. Zou, Z. Guan, H. Gurgenci, and Y. Lu, "Solar enhanced natural draft dry cooling tower for geothermal power applications," *Solar Energy,* vol. 86, no. 9, pp. 2686-2694, 2012.

[36] D. G. Kröger, *Air-cooled heat exchangers and cooling towers*. PennWell Books, 2004.

[37] S. IPSEpro, "Process Simulation Environment (PSE)," *Simtech, Austria,* 2003.

[38] V. Dostal, M. J. Driscoll, P. Hejzlar, and N. E. Todreas, "A supercritical CO2 gas turbine power cycle for next-generation nuclear reactors," *Proc. of ICONE,* vol. 10, p. 2002, 2002.

[39] S. M. Besarati and D. Y. Goswami, "Analysis of advanced supercritical carbon dioxide power cycles with a bottoming cycle for concentrating solar power applications," *Journal of Solar Energy Engineering,* vol. 136, no. 1, p. 010904, 2014.

[40] S. H. Yoon, J. H. Kim, Y. W. Hwang, M. S. Kim, K. Min, and Y. Kim, "Heat transfer and pressure drop characteristics during the in-tube cooling process of carbon dioxide in the supercritical region," *International Journal of Refrigeration,* vol. 26, no. 8, pp. 857-864, 2003.

[41] E. W. Lemmon, M. L. Huber, and M. O. McLinden, "NIST reference fluid thermodynamic and transport properties–REFPROP," ed: version, 2002.

[42] S. Duniam, "Design optimisation of an Australian EGS power plant using a natural draft dry cooling tower," 2016.

[43] X. Li, H. Gurgenci, Z. Guan, and Y. Sun, "Experimental study of cold inflow effect on a small natural draft dry cooling tower," *Applied Thermal Engineering,* vol. 128, pp. 762-771, 2018.

[44] Z. Zou, Z. Guan, and H. Gurgenci, "Optimization design of solar enhanced natural draft dry cooling tower," *Energy conversion and management,* vol. 76, pp. 945-955, 2013.

[45] A. E. Conradie, "Performance optimization of engineering systems with particular reference to dry-cooled power plants," Stellenbosch: University of Stellenbosch, 1995.

[46] M. Sadafi, I. Jahn, and K. Hooman, "Cooling performance of solid containing water for spray assisted dry cooling towers," *Energy Conversion and Management,* vol. 91, pp. 158-167, 2015.

[47] M. Sadafi *et al.*, "An investigation on spray cooling using saline water with experimental verification," *Energy conversion and management,* vol. 108, pp. 336-347, 2016.

[48] A. M. S. Alkhedhair, "Modelling and experimental study of spray cooling systems for inlet air pre-cooling in natural draft dry cooling towers," 2015.